JOURNAL OF SOLID STATE CHEMISTRY 54, 10–28 (1984)

The Monophosphate Tungsten Bronzes with Pentagonal Tunnels ($MPTB_P$), $P_4O_8(WO_3)_{2m}$: A High-Resolution Electron Microscopy Study

B. DOMENGÈS, M. HERVIEU, AND B. RAVEAU

Laboratoire de Cristallographie, Chimie et Physique des Solides, L.A. 251, ISMRA-Université, 14032 Caen Cedex, France

AND R. J. D. TILLEY

University of Cardiff, Cardiff-CF2 ITA-England

Received November 2, 1983; in revised form November 9, 1983

A series of monophosphate tungsten bronzes of composition $P_4O_8(WO_3)_{2m}$ with pentagonal tunnels, $MPTB_P$, have been investigated by high resolution electron microscopy. Most of the micrographs of the integral m members exhibit an asymmetrical contrast which could not be explained qualitatively by the structural models derived from X-ray diffraction studies of some members of the series. Image calculations were thus performed on the $m = 4$ member ($P_4W_8O_{32}$), which showed that the unexpected symmetry does not result from a structural anomaly, but could be due to a tilted electron beam. The observations revealed that ordered crystals can be obtained up to $m = 16$. The investigation of the nonintegral m compositions showed two sorts of intergrowths: disordered intergrowths of different m members belonging to the $MPTB_P$ series and ordered intergrowths of the $MPTB_P$ structure with a related phosphate tungsten bronze structure based upon hexagonal tunnels.

Introduction

Within the oxygen-rich region of the P–W–O system, two different series of phases both possessing the general formula $P_4O_8(WO_3)_{2m}$ have recently been reported (*1–5*). For these mixed valence tungsten oxides the corner-sharing PO_4 tetrahedra and WO_6 octahedra form a framework, which delimits empty tunnels, running through the WO_3-like matrix. The first type is obtained for $m = 3$ ($P_8W_{12}O_{52}$). Its framework is built up from P_2O_7 groups and WO_6 octahedra and is characterized by ReO_3-type columns limited by hexagonal tunnels. The second type corresponds to a large family, called the monophosphate tungsten bronzes, $MPTB_P$, which form a continuous series of microphases from $m = 4$ to 11 (*5*), characterized by ReO_3-type slabs connected through planes of "PO_4" tetrahedra forming pentagonal tunnels. The later family is rather complex, for instance, the members $m = 4$ and 6 whose structures have been resolved by X-ray diffraction have uniform slab widths, while the member $m = 5$, corresponds to the intergrowth of slabs of the $m = 4$ and 6 phases.

A recent analysis of this structure (*6*) has shown that it is closely related to that of the $MPTB_H$ bronzes $K_xP_4O_8(WO_3)_{2m}$ and $Na_xP_4O_8(WO_3)_{2m}$ (*6, 7*), which exhibit the same ReO_3-type slabs and phosphate planes, but linked so as to form hexagonal

0022-4596/84 $3.00

tunnels. It would seem possible, therefore, that the $P_4O_8(WO_3)_{2m}$ series may also exist in two forms, one as already described with pentagonal tunnels and one with hexagonal tunnels. This view is reinforced when the γ and η structures of the oxide Mo_4O_{11} are considered (*8, 9*). These structures are identical, respectively, with the expected $MPTB_P$ and $MPTB_H$ structures for the m = 6 member of the series, except for the replacement of W and P by Mo. To date, though, no clearly dimorphic oxides of the $P_4O_8(WO_3)_{2m}$ series have been observed. Nevertheless anomalous electron diffraction contrast noted in a preliminary electron microscope study of these materials (*5*) may reveal an alternative method of linking WO_3-like regions with phosphate groups.

The aim of the present study was to clarify some of the uncertainties in the crystal chemistry of these phases posed by the previous studies. These may be listed as, first, a study of the anomalous contrast previously reported to determine its significance, second, to investigate the nonintegral m values and high m values terms in the series to complete earlier studies, and third, to search for possible existence of $MPTB_H$ structures in $MPTB_P$ materials. The results of the investigations are presented in this paper.

Experimental

The samples of different compositions used in this investigation were prepared as previously described (*1–5*). Long annealing times were employed for the preparations corresponding to the highest m values. For electron microscope observation, they were ground in an agate mortar, suspended in *n*-butanol, and collected on a perforated carbon grid. Electron diffraction patterns and lattice images were obtained on a JEM 100CX electron microscope operated at 120 kV. Thin crystal regions were aligned with a goniometer (top entry) stage so as to give (*Okl*) reciprocal lattice sections and the images were recorded by using an objective aperture with a radius of 0.42 $Å^{-1}$ in reciprocal space.

Images were calculated using the multislice method and programs FCOEFF and DEFECT written by Skarnulis (*10*). Through-focal series of images were calculated for different crystal thicknesses using the parameters: spherical aberration constant C_s = 0.7 mm, depth of focus = 170 Å, incident beam convergence = 0.1 mrad.

The Structure of $MPTB_P$

The structure of the MPTB phases, observed in the P–W–O and *A*–P–W–O sys-

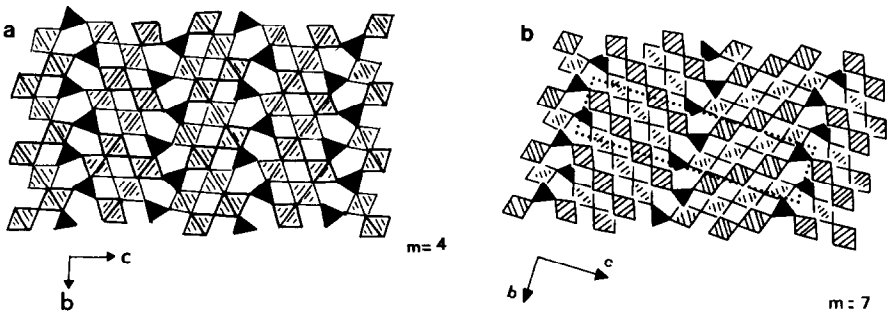

FIG. 1. Projection onto (100) of the orthorhombic cell of the $P_4O_8(WO_3)_{2m}$ structure: (a) even-m member, m = 4, (b) odd-m member, m = 7.

TABLE I

CRYSTALLOGRAPHIC DATA FOR $MPTB_P$-TYPE $P_4O_8(WO_3)_{2m}$ PHASES

m	Composition	a (Å)	b (Å)	c (Å)
4	$P_4O_8(WO_3)_8$	5.285(2)	6.569(1)	17.351(3)
6	$P_4O_8(WO_3)_{12}$	5.296(2)	6.567(3)	23.575(8)
7	$P_4O_8(WO_3)_{14}$	5.299(5)	6.561(4)	26.648(11)
8	$P_4O_8(WO_3)_{16}$	5.301(2)	6.554(5)	29.711(15)
9	$P_4O_8(WO_3)_{18}$	5.303(3)	6.551(4)	32.800(15)
10	$P_4O_8(WO_3)_{20}$	5.306(4)	6.549(5)	35.952(14)
11	$P_4O_8(WO_3)_{22}$	5.310(5)	6.543(7)	39.014(19)

tems (A^+ = K^+, Na^+) has been described fully in recent publications (*2, 4–7*) and will only be discussed briefly here. As shown in Fig. 1 the framework of the structure is composed of ReO_3-type slabs of equal thickness. Each slab is characterized by strings of $m/2$ octahedra extending along the [001] direction of the ReO_3 lattice, or by strings of m octahedra along the [110] direction. These strings are limited at each end by a PO_4 tetrahedron. The tetrahedra lie on planes and form the connection between successive ReO_3-type slabs. The corner-sharing tetrahedra and octahedra delimit pentagonal tunnels running along the "b" axis and located in the planes of PO_4 tetrahedra, which can be called "phosphate" planes. The strings of m octahedra are inclined at ±35° with respect to the "b" axis, i.e., to the tunnel rows. These phases are found to crystallize in the orthorhombic system with space group $P2_12_12_1$ for the even-m members and space group $P2nn$ for the odd-m members. Table I lists the lattice parameters of some previously identified phases in this series (*5*).

The m = 5 member of the family (*2*) appears as an exception: its host lattice is also built up from ReO_3-type slabs connected through PO_4 tetrahedra in the same way but two successive slabs have a different width corresponding to two and three octahedra (along $[001]_{ReO_3}$), so that the structure can be considered as an intergrowth of the integral members m = 4 and m = 6 (Fig. 2). It cristallizes in the monoclinic system with a = 6.566 Å, b = 5.285 Å, c = 20.573 Å, β = 96°18, and space group $P21$.

Results

Problems of Contrast: Image Matching

Provided that a number of particular imaging conditions are fulfilled the electron micrograph contrast taken under high resolution imaging conditions can be a representation of the charge density within the crystal projected in the direction of the electron beam. X-Ray crystal structure determinations of the phases investigated here showed that, appart from the mirror-image effect due to the twinned nature of the ReO_3-like slabs, each phosphate plane and sheet of tunnels was identical. Thus electron micrographs taken under the correct high resolution imaging conditions should show identical contrast at the positions corresponding to the tunnel planes. In practice only a small number of crystals exhibited the expected contrast. Micrographs of such crystals are shown in Fig. 3, for the phases with m = 4 and 8. From a comparison with the structure of $P_4W_8O_{32}$ (m = 4), it can be seen that the rows of white spots correspond to the empty pentagonal tunnels, whereas the weaker white broad lines

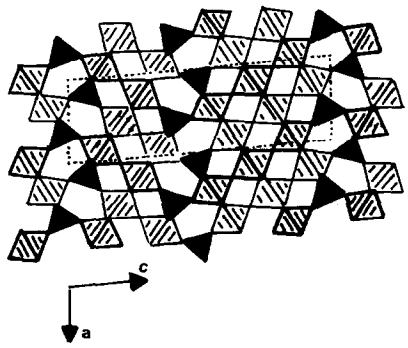

FIG. 2. Projection onto (100) of the monoclinic cell of $P_4W_{10}O_{38}$ (m = 5).

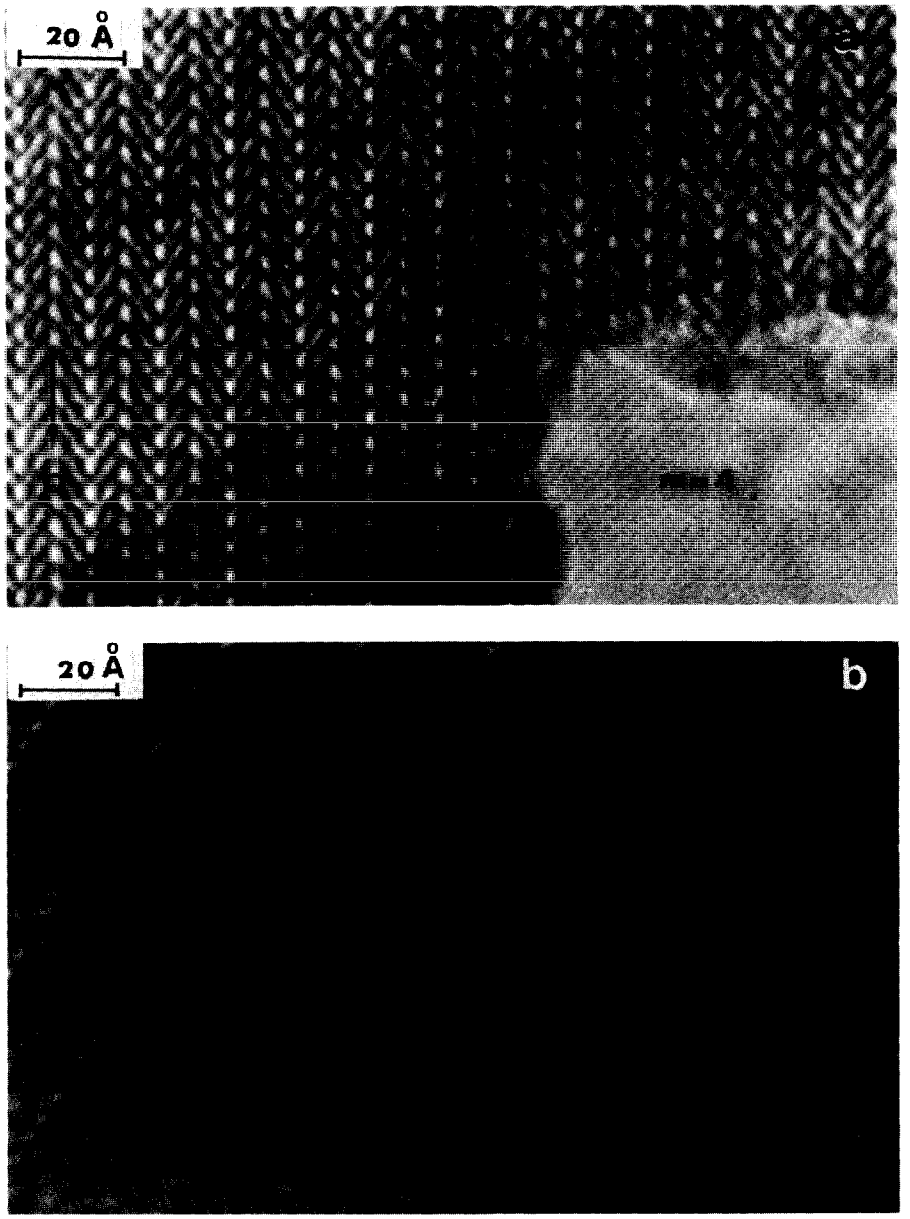

FIG. 3. Electron micrographs of crystals oriented with [100] parallel to the electron beam. (a) $m = 4$, (b) $m = 8$.

inclined at ±35° with respect to these rows correspond to the rhombic tunnels.

In contrast to this, most crystal fragments exhibited a quite different form of contrast, illustrated in Fig. 4, which shows images from crystal fragments of phases with $m = 4$, 9, and 11. It can be seen from these micrographs that the rows of spots corresponding to the pentagonal tunnels exhibit alternately a bright and dark contrast.

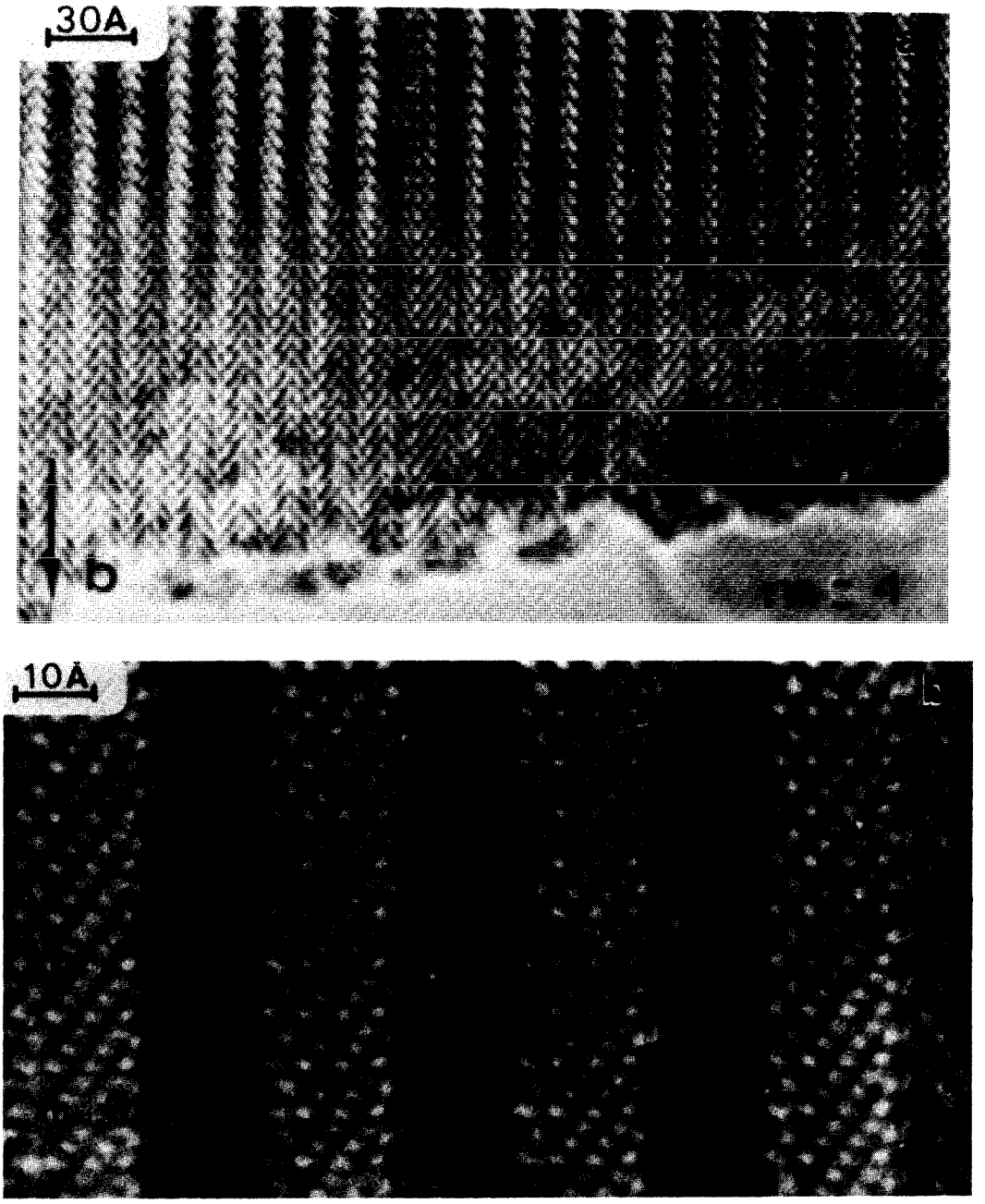

FIG. 4. Electron micrographs of fragments of crystals exhibiting uneven contrast; (a) $m = 4$, (b) $m = 9$, and (c) $m = 11$.

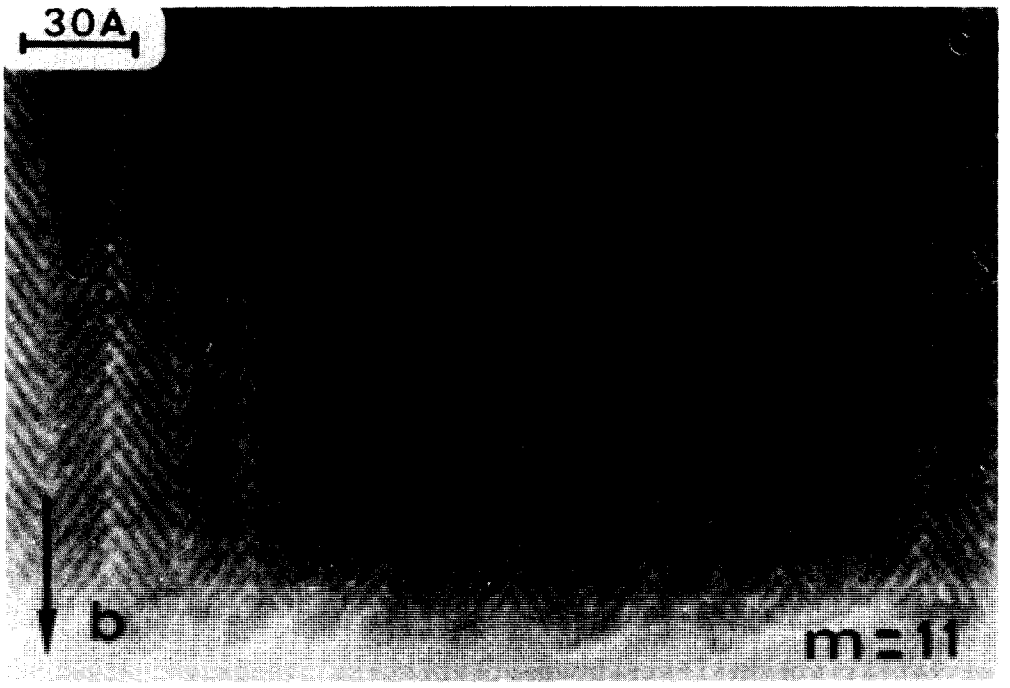

FIG. 4—*Continued.*

Moreover we observed that the contrast was very sensitive to the crystal tilt away from the symmetrically excited (100) zone and to the crystal thickness as illustrated in Fig. 5. The variation of the intensity of the spots from one tunnel row to the other which is very weak, almost undiscernible, in the thinnest area of the crystal edge, increases as the thickness of the crystal increases and finally disappears in the thickest part of the crystal.

This unexpected contrast raised a number of questions. The most important of these, by far, was whether the anomalous contrast was caused by a new structure, so that each phosphate plane was not identical to each other plane but instead pairs of planes with different structures were found in some crystals. Although this idea was not entirely reasonable chemically, it was still a possibility.

In order to investigate this and other suggestions systematically, image calculations were performed for the $m = 4$ member, $P_4W_8O_{32}$, using the atomic coordinates obtained by X-ray diffraction (*4*). A large number of through-focal series were first computed for different crystal thicknesses; the results for a crystal 26.5 Å thick are shown in Fig. 6. It is clear that the calculated images agree with the micrograh of Fig. 3. Moreover these image calculations showed that any difference of intensity between the successive rows could not be simulated, irrespective of the values of the parameters used. Results were in accordance with the projected potential, and especially the contrast of two adjacent rows of pentagonal tunnels parallel to *b* are always similar. Thus it appears that the contrast variations observed for many crystal are not due to thickness effects alone, or simple variations in electron optical conditions.

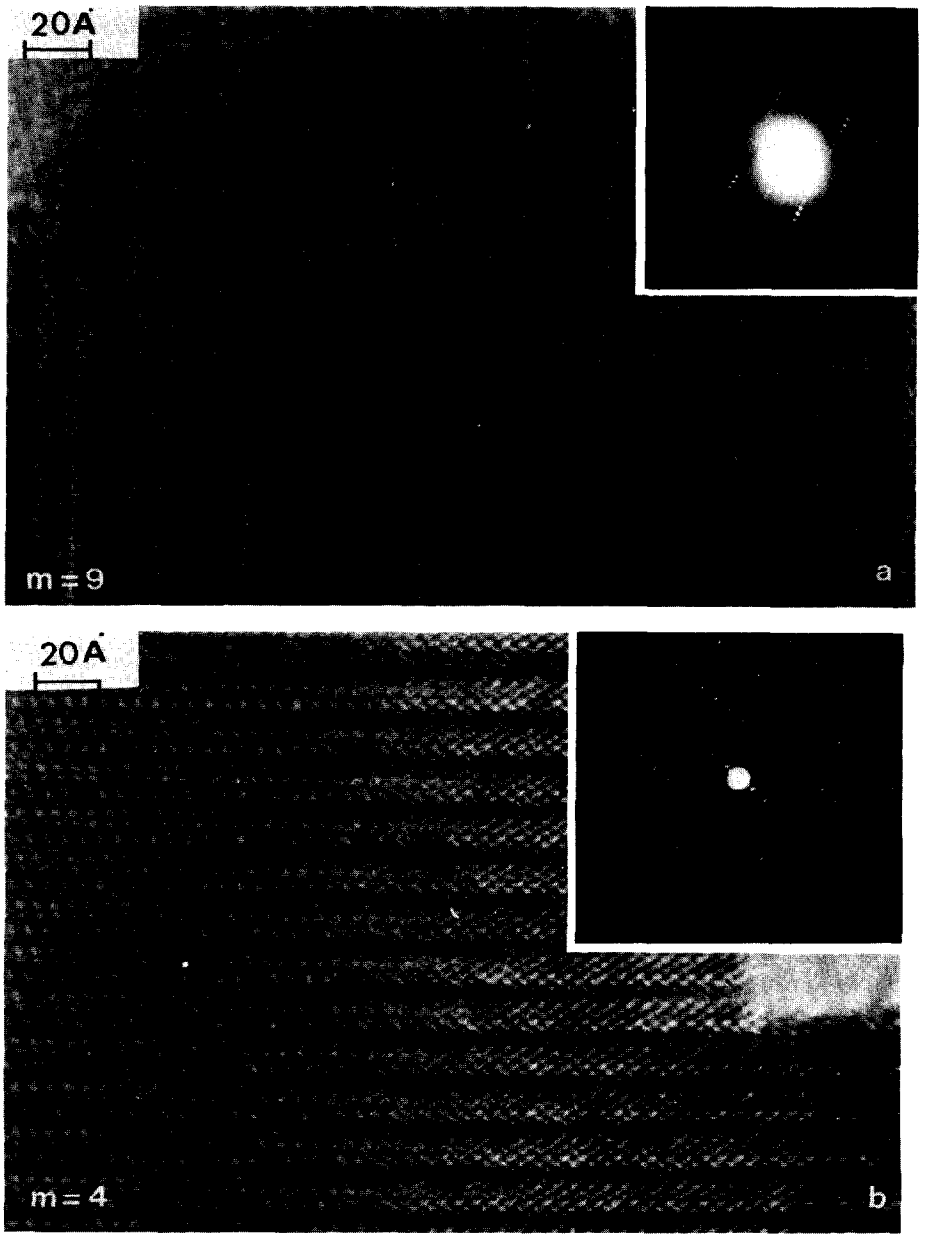

FIG. 5. Electron micrographs of fragments of (a) $m = 9$ and (b) $m = 4$ crystals. Note the variation in symmetry of contrast with thickness.

Theoretical studies in the past have also indicated that misalignment of the electron beam with respect to the optical axis of the electron microscope or the crystal itself can also produce image degradation (*12, 14*). To take this possibility into account we included a small beam tilt in the calculations. Through-focal series were calculated for

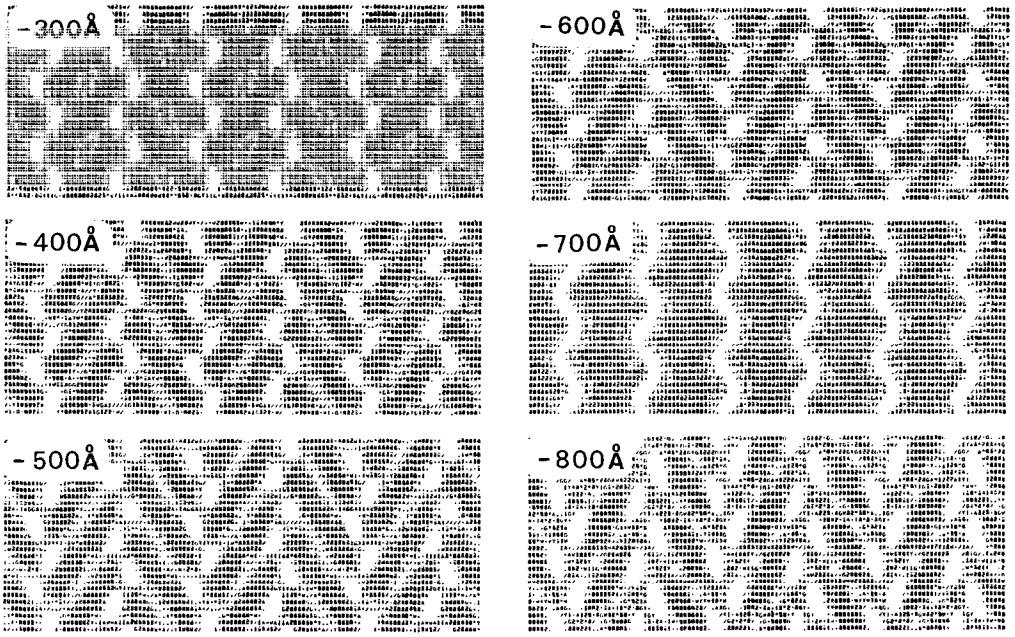

FIG. 6. A calculated series of images for a $P_4W_8O_{32}$ crystal, using a crystal thickness of 27 Å.

various crystal thicknesses and beam tilts with respect to the crystal zone axis. The calculated images were proved to be very sensitive to beam tilt and lead to satisfactory results. Good agreement between the experimental and the simulated images were obtained by positioning the center of the Laue-circle at $X = Y = 0.22$, corresponding to a tilt of 1.2 mrad. Figure 7 shows the calculated images for 26.5, 90.1, and 132.5 Å crystal thickness with and without beam tilt. It is seen that in thin regions the difference of intensity between two successive rows of white spots is very small, especially in the optimum focus image. It increases as the thickness increases and is maximum for the 90.5-Å-thick image where one tunnel row out of two appears as white spots whereas the other one is weaker or quite absent. For the 132.5-Å-thick crystal, the intensities of the white spots are still different from one tunnel row to the other but it is noted that the difference is smaller in such images in agreement with our observations.

These preliminary calculations are a first approach in understanding the experimental results. Further experiments and calculations are obviously necessary before a clear understanding of the asymmetrical contrast is achieved. They have served to prove, however, that the unusual contrast effects observed were not caused by structural changes associated with the rows of tunnels or the linkage of these tunnels with their neighboring ReO_3-type slabs. Instead the observed contrast variations could be explained as expected in terms of illumination tilt with respect to the optical axis. Further work, both experimental and theoretical will be necessary before all aspects of the problem are completely understood, and these studies are planned for the future.

High and Nonintegral "*m*" Compositions—Intergrowths

High resolution electron microscopy confirmed the existence, for $4 \leq m \leq 11$ ($m \neq 5$), of a series $P_4O_8(WO_3)_{2m}$ built up from

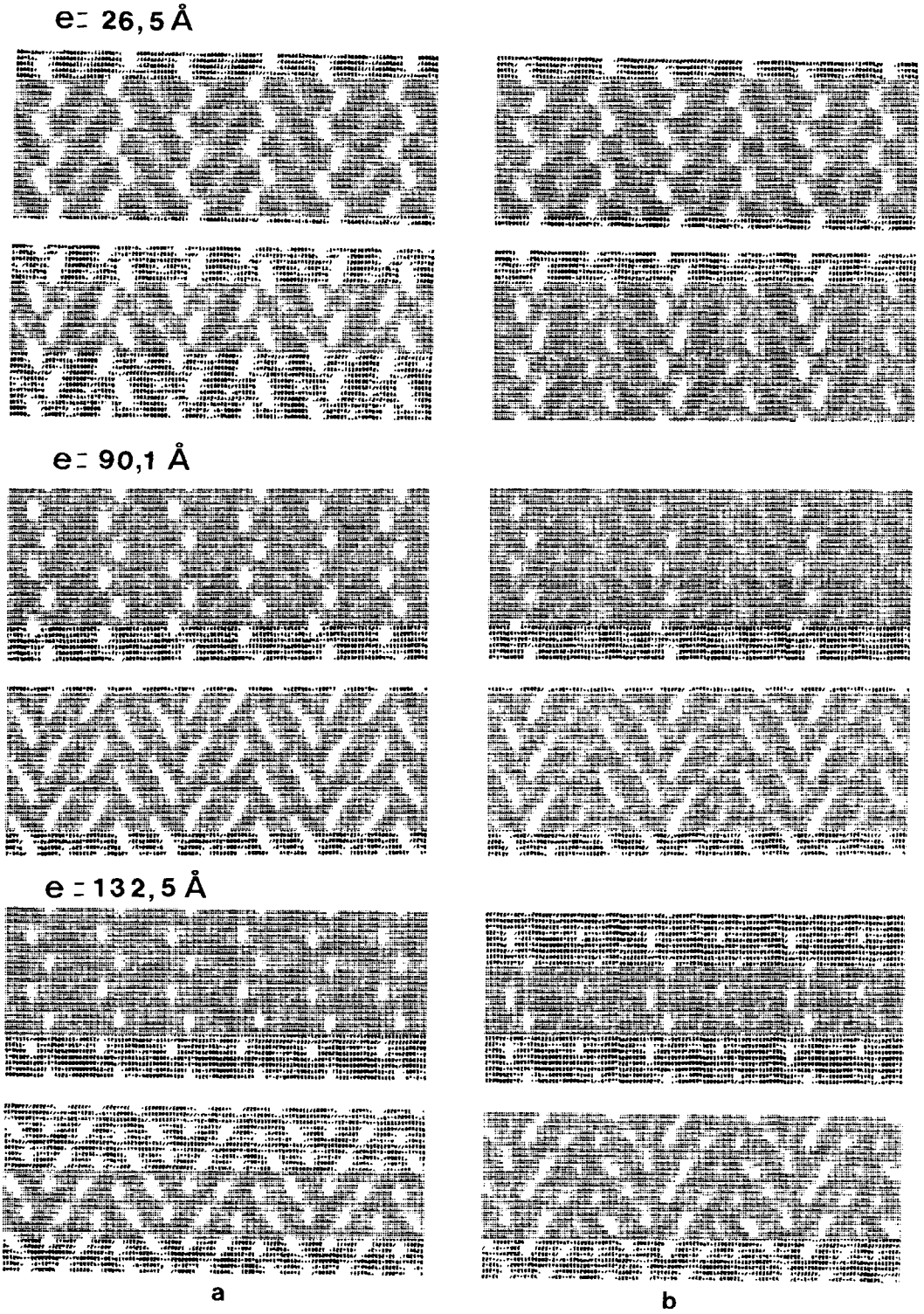

FIG. 7. Calculated images of $P_4W_8O_{32}$ for crystals thicknesses of 26.5, 90, and 132.5 Å. (a) Without beam tilt, (b) beam tilt of 1.2 mrad.

ReO_3-type slabs separated by planes of PO_4 tetrahedra forming empty pentagonal tunnels [(5) and this work]. The investigation of the highest m values showed that regular microcrystals, characterized by widest ReO_3-type slabs, could be isolated as regular microphases, with $12 \leq m \leq 16$; they were identified by their electron diffraction patterns and their electron microscope images.

Such members as $m = 12$, 13, 15, and 16 are shown in Fig. 8. A large number of different crystal fragments were analyzed; these observations showed that crystals corresponding to integral m values ($m \leq 11$) exhibit a great regularity in the distribution of "PO_4"-plane spacings; only few different spacings have been observed with m' values different from that of the nominal composition. Figure 9 shows such defects arising in a crystal of $m = 4$ nominal composition. One of these is a slab of 7 octahedra in a "$m = 4$" matrix and the other consists of successive slabs of five octahedra in this matrix. It is of interest to note that the member $m = 5$ corresponding to this microphase has never been synthesized; this composition being an intergrowth of the members $m = 4$ and $m = 6$.

For the nonintegral lowest values of m, $4 \leq m \leq 11$, the results obtained from both the electron diffraction study and the X-ray diffraction investigation indicated that the samples consist of mixtures of various m-value crystals, with m usually close to that of the nominal composition. For the nonintegral highest values of m, i.e., $m > 11$, the X-ray powder patterns exhibit many very diffuse diffraction lines. The electron diffraction study allowed two types of microcrystals to be identified, viz. regular microcrystals already described and strongly disordered crystals, characterized by streaked lines parallel to the "c" axis. Lattice images of these crystals in most cases showed a wide variation in the spacings of the PO_4 planes, corresponding to the disordered intergrowth of various $MPTB_P$ members. Figure 10 shows that the width of the ReO_3-type slabs can vary drastically; so, for a nominal composition $m = 13.6$, ReO_3-type slabs of $m = 2$ to $m = 17$ are intergrown and sometimes adjacent. In this image, it must be noted that some slabs of 2, 3, and 5 octahedra are stabilized and the 17-octahedra-width slab can be regarded rather as a WO_3 domain since no member $m = 17$ has been identified.

Presence of Hexagonal Tunnels in the $MPTB_P$ Matrix–Intergrowth of $MPTB_P$ and $MPTB_H$

The comparison of the structures of the $MPTB_P$ $P_4O_8(WO_3)_{2m}$ oxides with those of the $MPTB_H$, $A_xP_4O_8(WO_3)_{2m}$ (A = K, Na) oxides has shown that both structures are formed of identical mixed layers of octahedra and tetrahedra (6) as shown for instance in Fig. 11a. For $m = 4$ these layers can be associated to form either distorted hexagonal tunnels (Fig. 11b) or pentagonal tunnels (Fig. 11c), so that the $MPTB_H$ and $MPTB_P$ structures only differ one from the other by the stacking of those mixed layers. Hence the $MPTB_P$ structure can be derived from the $MPTB_H$ structures simply by rotation of one mixed layer out of two by 180° around the a axis. The presence of the A ions does not seem necessary to stabilize the $MPTB_H$ structure since the two Mo_4O_{11} forms, γ and η, described by Magnéli and Kihlborg (8, 9) exhibit, respectively, the $MPTB_P$ and $MPTB_H$ structure, but contain empty tunnels.

Different attempts to synthesize $MPTB_H$ microphases in the $P_4O_8(WO_3)_{2m}$ oxides have been unsuccessful up to the present time. However, HREM observations showed that this structure appears in the form of defects in a great number of crystals. This type of defect has been labeled M, because the cell which characterizes the $MPTB_H$ series, shown in Fig. 12 (black ar-

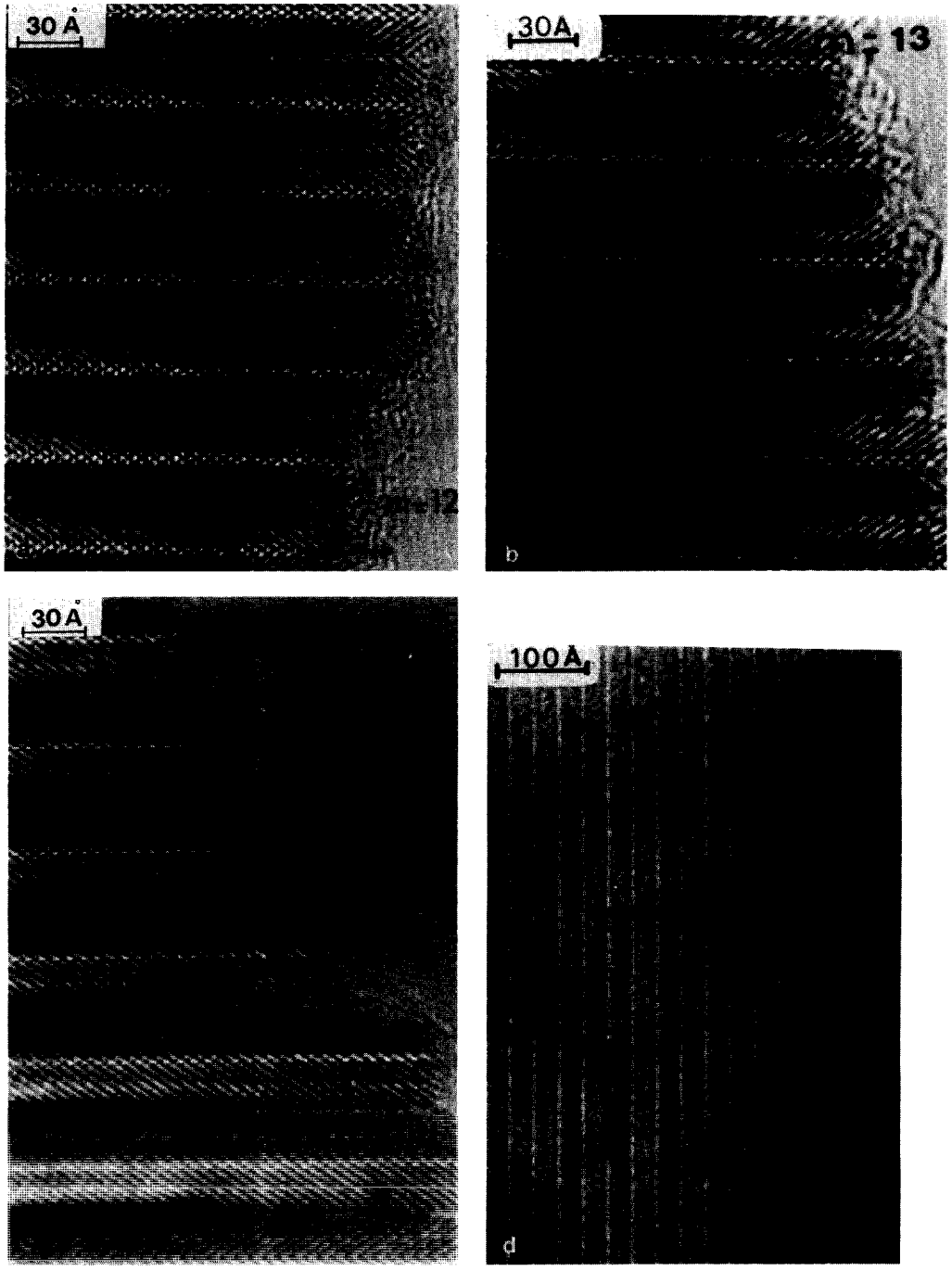

FIG. 8. The highest m value members of the $P_4O_8(WO_3)_{2m}$ series with the $SPTB_P$ structure. (a) m = 12, (b) m = 13, (c) m = 15, (d) m = 16.

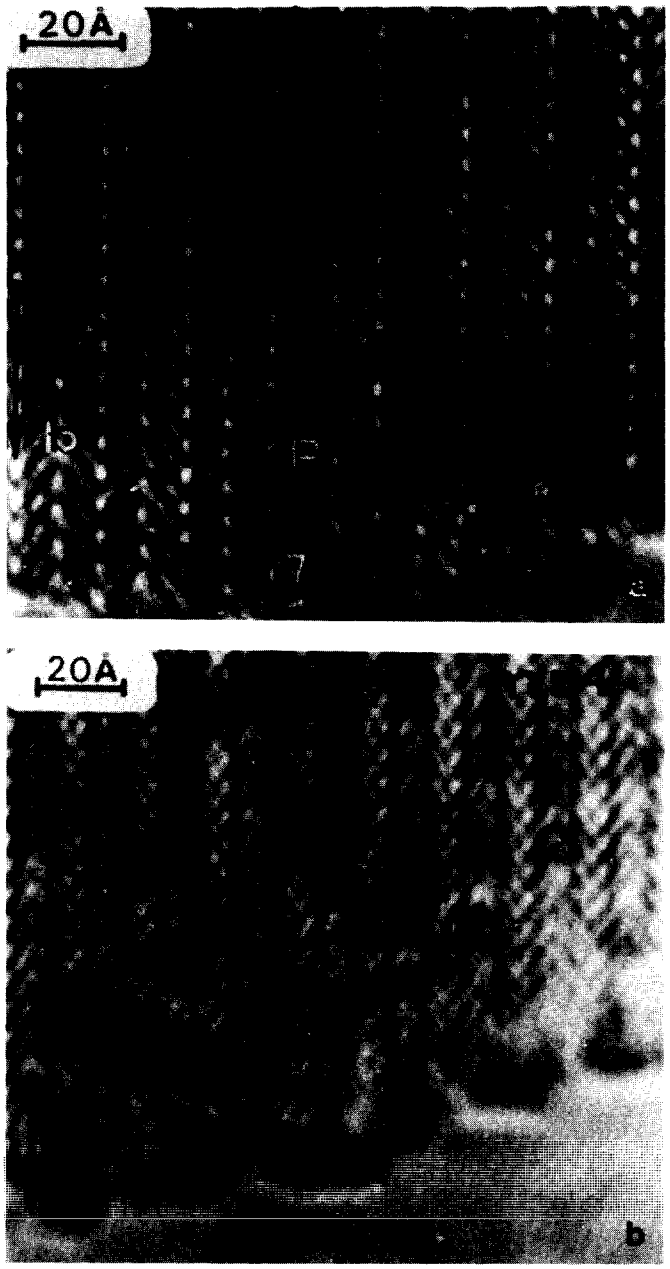

FIG. 9. Occurrence of $m = 7$ slab (a) and an $m = 5$ member (b) in a matrix of nominal composition $m = 4$.

rows), is monoclinic. The nominal composition of the sample corresponds to $m = 14$. On this micrograph, the empty hexagonal tunnels appear as white dots, spaced about 6.6 Å apart instead of 3.3 Å for the pentagonal tunnels. The white lines of the rhombic ReO_3-type tunnels remain parallel on both sides of the defect and appear in alternate

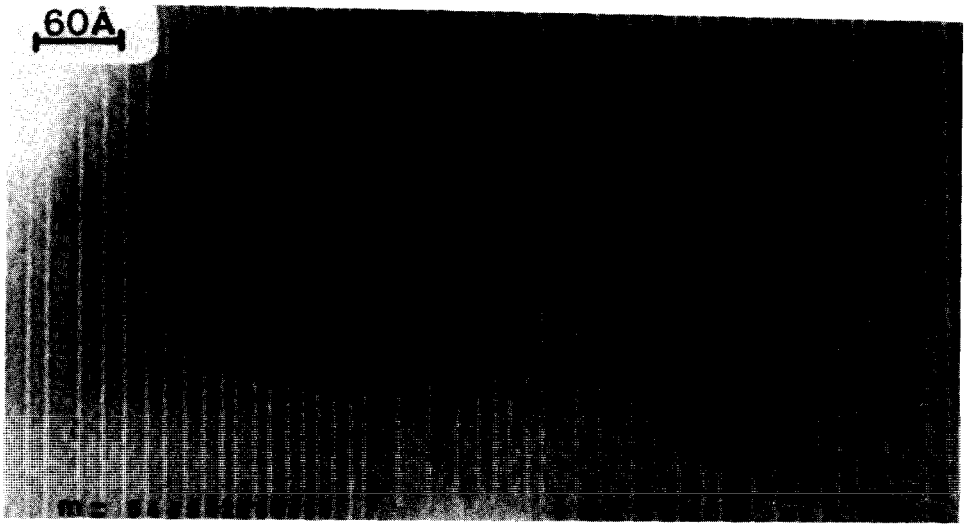

FIG. 10. Low resolution image of a strongly disordered crystal with nominal composition $m = 13.6$.

rows in accordance with the idealized drawing of the structure. Figure 12b presents an interpretation of the image contrast near the defect. Such a defect can be regarded as a localized intergrowth of the two structural $MPTB_P$ and $MPTB_H$, symbolized as (. . P m H m' P . . .), where H and P correspond, respectively, to the hexagonal and pentagonal tunnel rows in the PO_4-planes and which ensures that the junction between the ReO_3-type slabs of m and m' octahedra is formed with a minimum of misfit. The M defect was mostly observed in the middle of a ReO_3-type slab for high m values ($m = 9$). Some sequences of 2, 3, or 4 M defects occurred, as those shown in Fig. 13.

An other observation which was frequently made is illustrated in Fig. 14. This shows very regular sequences occurred in the microcrystals leading to ordered intergrowths between the $MPTB_P$ and $MPTB_H$ structures. In the microcrystal of nominal composition $m = 14.66$, shown in Fig. 14 "M" defects appear in a regular manner nearly in the middle of the ReO_3-type slabs. The new microphase could be formally described as

$$P(14 - n)\ H(n - 1)\ P(n' - 1)\ M(14 - n')$$

where n and n' characterize the widths of the octahedral slabs. It is noted that the "PO_4" plane of the defect replaces a row of

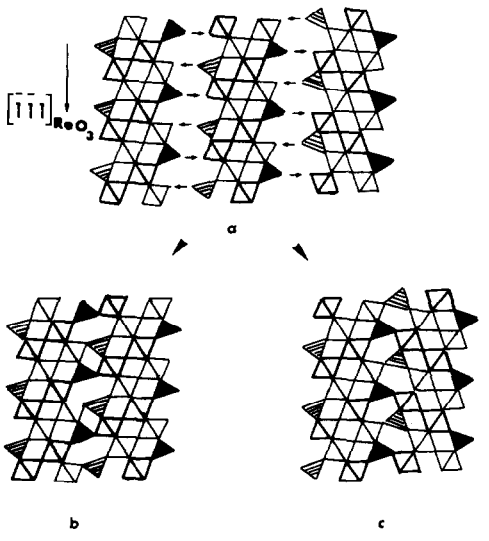

FIG. 11. Idealized drawing of mixed layers (a) of octahedra and tetrahedra which can be associated to form $MPTB_H$ (b) and $MPTB_P$ (c) structures.

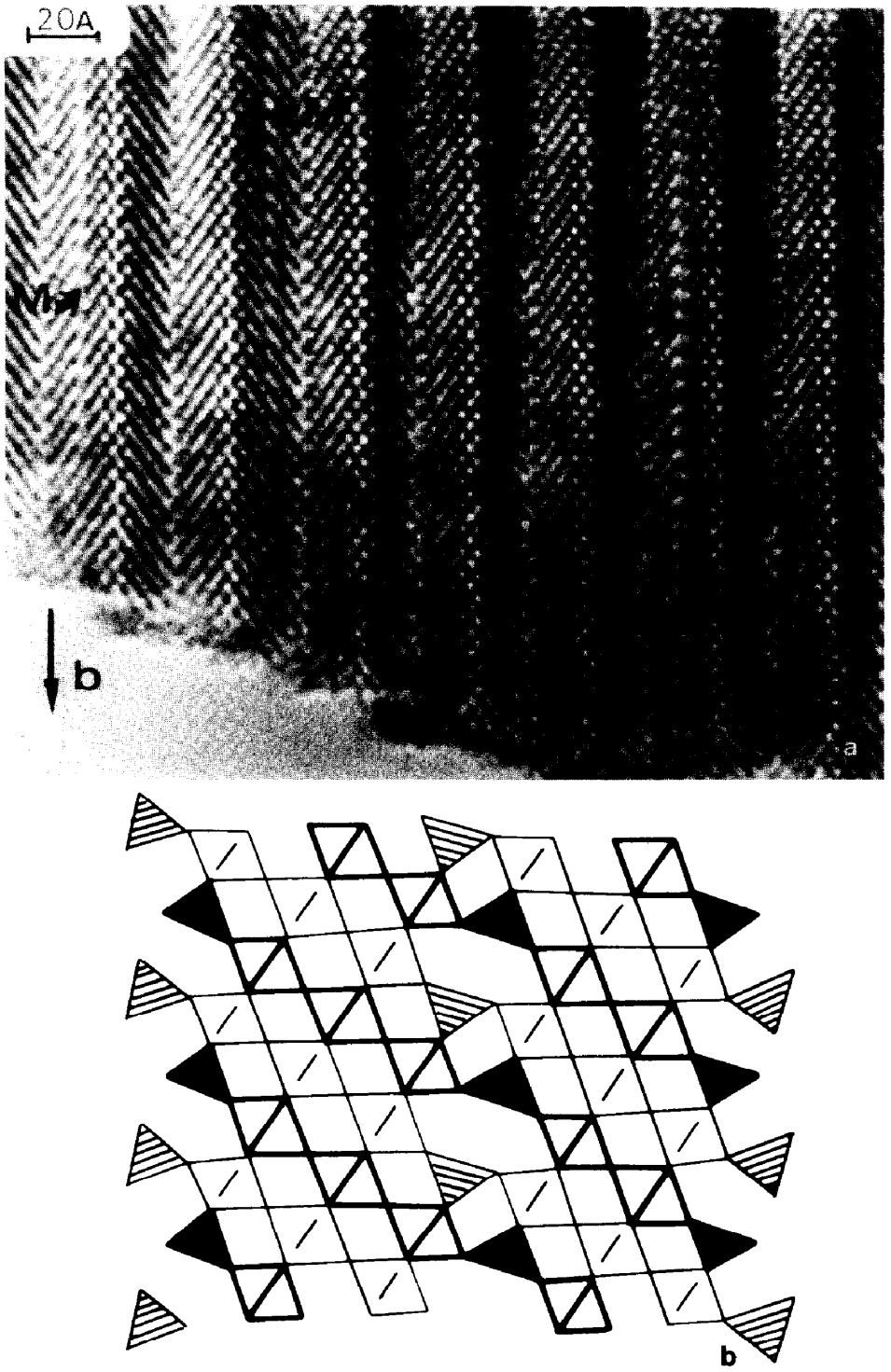

FIG. 12. (a) Lattice image of an $m = 14$ crystal showing a defect of M type. (b) Idealized drawing projected along $[\bar{1}10]_{ReO_3}$ of the defect.

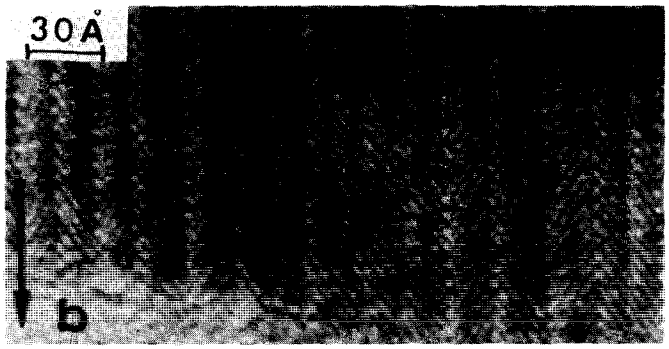

FIG. 13. Lattice image of a microcrystal mainly of composition corresponding to $m = 11$, showing sequences of M defects.

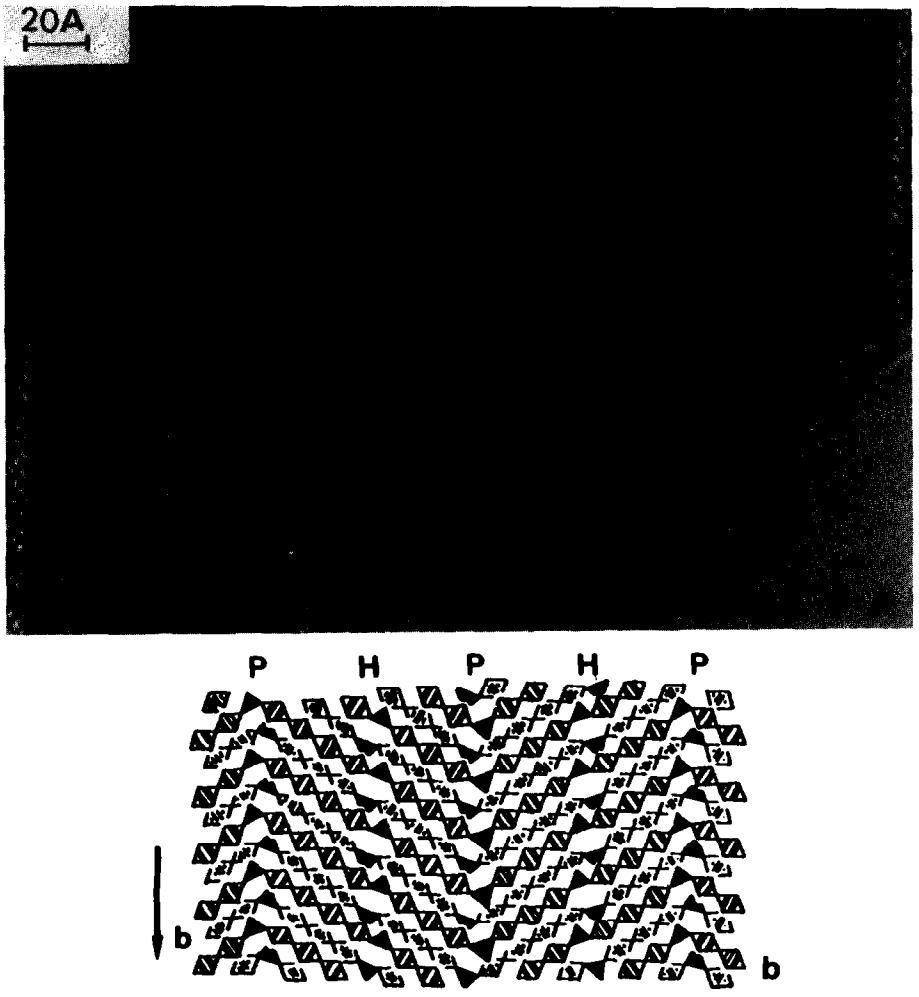

FIG. 14. Image of a crystal of nominal composition $m = 14.66$ exhibiting intergrowth of $MPTB_H$ and $MPTB_P$ structures (a) and the idealized projection (b).

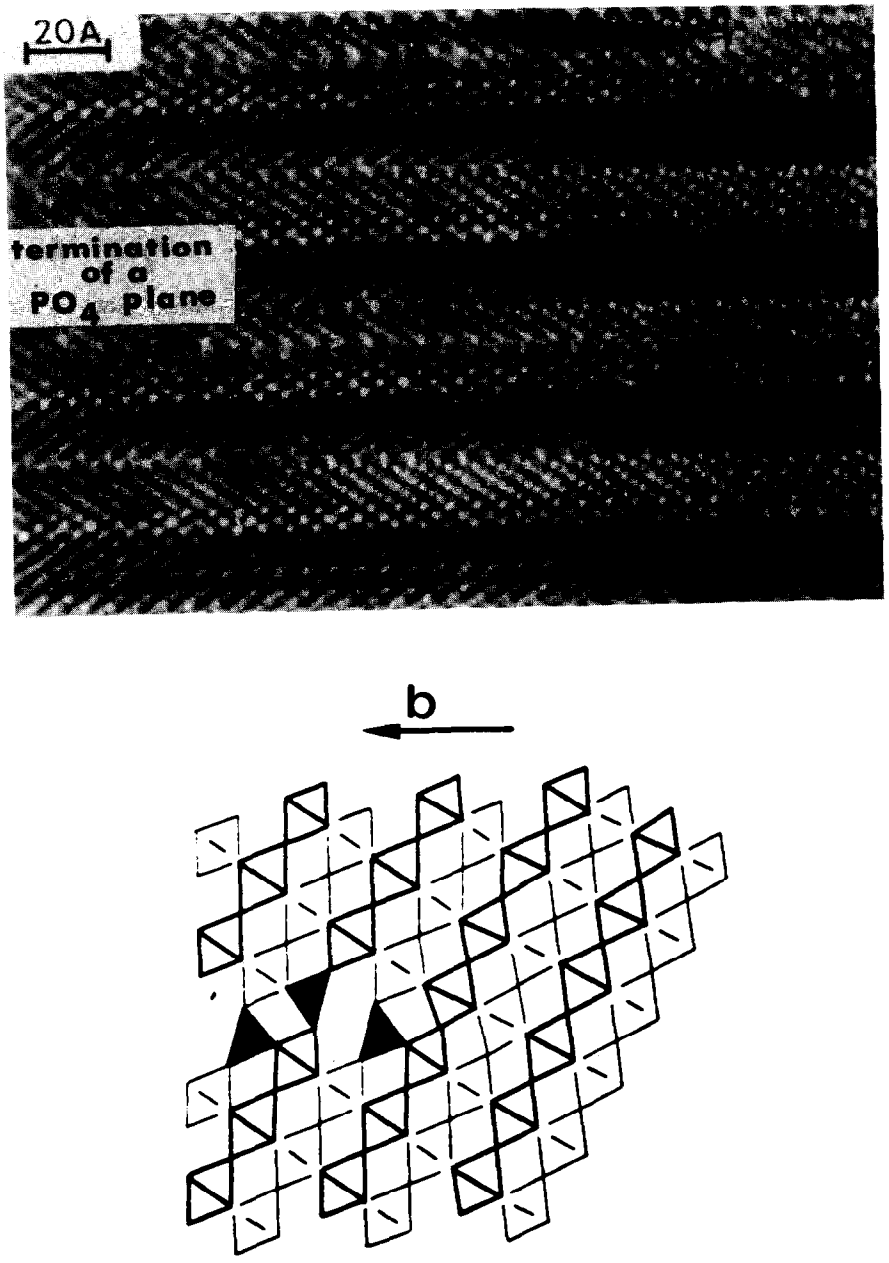

FIG. 15. (a) High resolution micrograph showing the termination of a "PO_4" plane in the crystal bulk of $P_4O_8(WO_3)_{18}$. (b) Interpretation of the defect.

octahedra and thus this microphase corresponds to a different local composition of the crystal fragment; the average composition of the crystal being $P_8O_{16}(WO_3)_{2(m-1)}$. The interpretation of this defect is shown in Fig. 14b.

This new type of junction of the octahedral ribbons by way of hexagonal tunnels

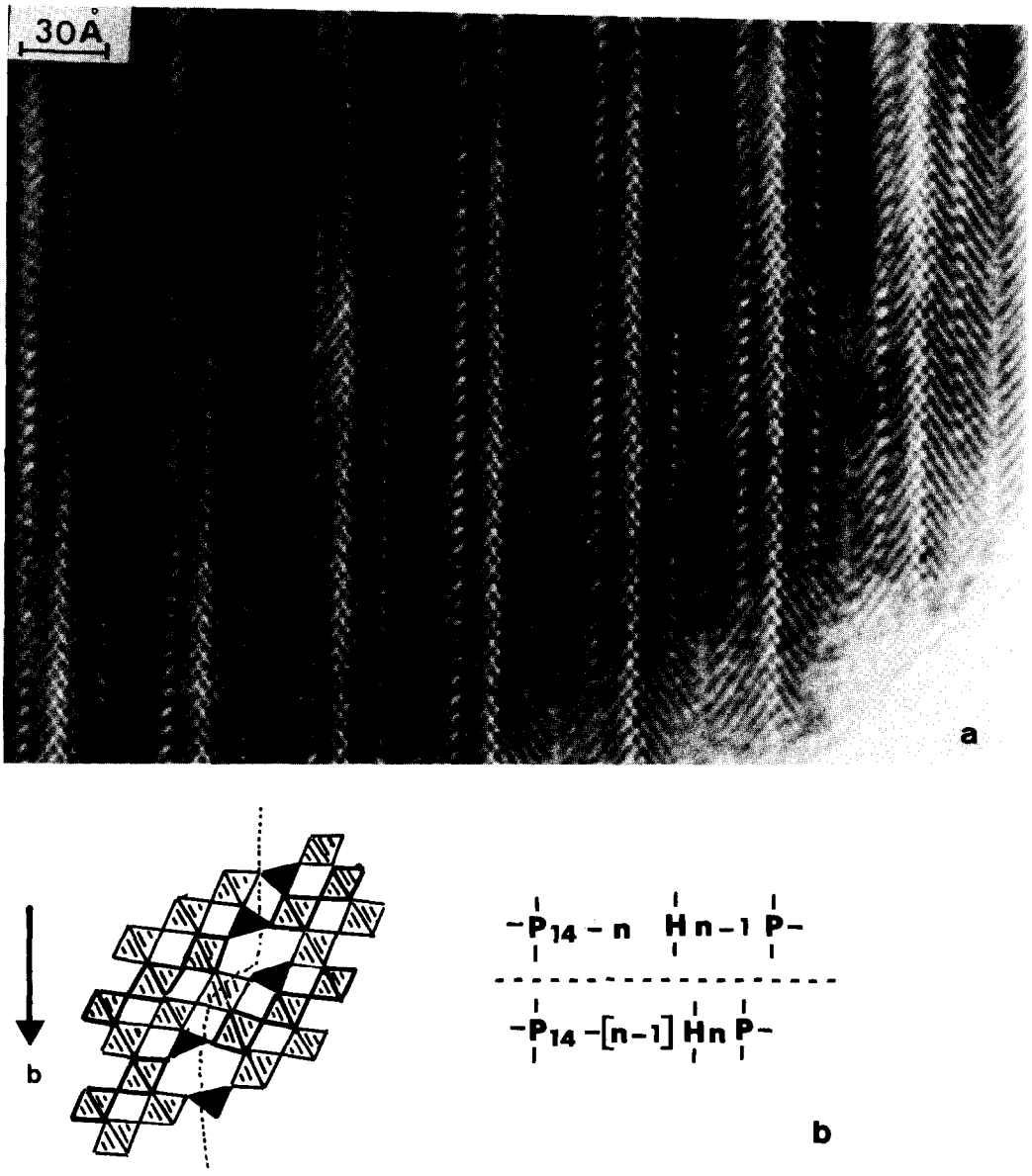

FIG. 16. $P_4O_8(WO_3)_{22}$: (a) micrograph of defects occurring in $MPTB_P$–$MPTB_H$ intergrowths, (b) an idealized drawing of these defects, (c) the interruption of the hexagonal tunnels row.

can lead to the formation of new types of defects. One of the most typical of them is the disappearance of the rows of hexagonal tunnels in the ReO_3-type slab as shown in Fig. 15a (black arrow). This defect can be interpreted as the termination of the extra "PO_4" plane, i.e., by the replacement of the PO_4 tetrahedra by WO_6 octahedra. An idealized drawing is shown in Fig. 15b. Such terminations of "PO_4" planes result from the characteristic structure of the starting $MPTB_H$-type defect where the oc-

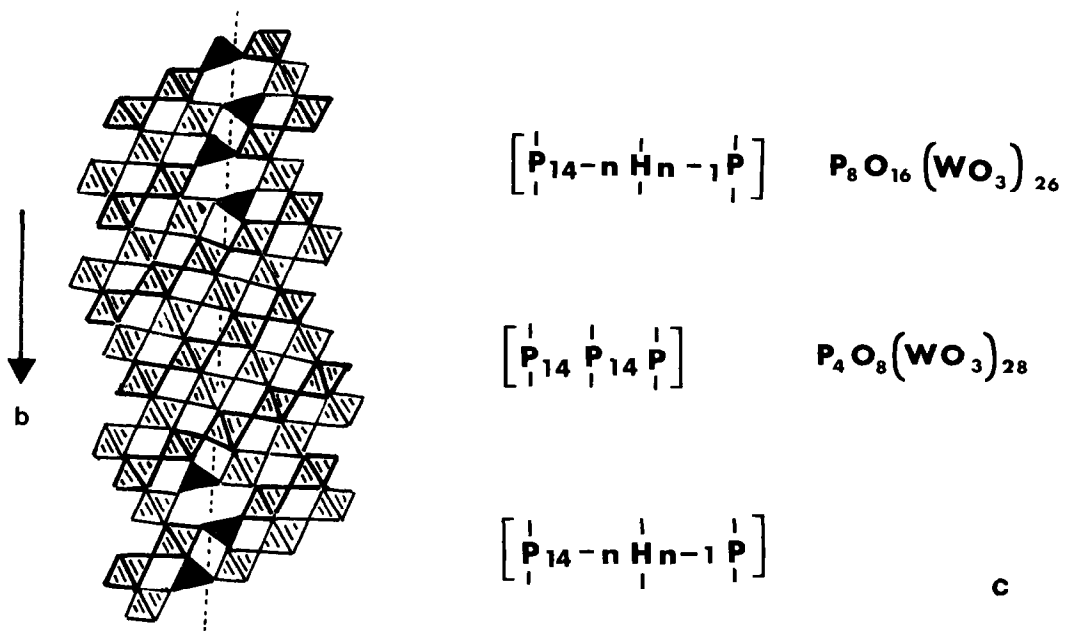

FIG. 16—*Continued.*

tahedral ribbons are parallel on both sides of the defect. The replacement tetrahedron–octahedron involves only a slight distortion of the host lattice, as shown on the micrograph and its interpretation.

Figure 16a shows a quite ordered intergrowth of $MPTB_P$ and $MPTB_H$ structures observed in a crystal flake with nominal composition $m = 11$. This area exhibits two new features. (1) The hexagonal tunnel row seems to be translated inside the ReO_3-type slab, involving a variation of the numbers $(n - 1)$ and $(14 - n)$ of octahedra on both sides of the tunnels row. This suggests that the substitution octahedron–tetrahedron is made in a direction different from that of the PO_4 plane (*b* axis) (Fig. 16b). This stopping and translation of the junction is usually observed with a shifting of one or two octahedra and leads to a swinging of the hexagonal tunnel row inside the ReO_3-type slab. (2) It is seen that some hexagonal tunnel rows disappear here and reappear, sometimes at exactly the same lateral position, sometimes with a translation (2′). This could result from isolated hexagonal tunnels in the middle of the octahedra slab. A model is proposed in Fig. 16c.

Finally we note that the defects described above seemed to be present in the original crystals and did not appear to arise as a result of damage due to the electron beam or other related effects. The influence of deliberate radiation damage would be of interest.

Conclusion

Electron micrographs of $MPTB_P$ crystals from the $P_4O_8(WO_3)_{2m}$ series of phases often exhibit an unexpected contrast. Image calculations show that this phenomenon does not result from a structural anomaly but can be simulated by introducing a small tilt into the illuminating electron beam. An investigation of the high nonintegral *m* compositions of these phases shows that the $MPTB_P$ structure can be stabilized with

wide ReO_3-type slabs up to 16 octahedra and that disordered intergrowths of $MPTB_P$ members, and ordered intergrowths of $MPTB_P$ and $MPTB_H$ structures are mainly responsible for the nonstoichiometry in this structural family. The absence of $MPTB_H$ microphases in the $P_4O_8(WO_3)_{2m}$ oxides is not understood at the present time. However, the possibility of formation of $MPTB_H$–$MPTB_P$ intergrowths in this system, and the existence of $A_xP_4O_8(WO_3)_{2m}$ (A = Na, K) phases with the $MPTB_H$ structure, lead us to suppose that the synthesis of regular intergrowths, and single $MPTB_H$ microphases may be governed by the alkali ion content in these materials. Investigations are being carried out in this direction.

References

1. B. DOMENGES, M. GOREAUD, PH. LABBE, AND B. RAVEAU, *Acta Crystallogr. Sect. B* **38,** 1724 (1982).
2. A. BENMOUSSA, PH. LABBE, D. GROULT, AND B. RAVEAU, *J. Solid State Chem.* **44,** 318 (1982).
3. J. P. GIROULT, M. GOREAUD, PH. LABBE, AND B. RAVEAU, *J. Solid State Chem.* **44,** 407 (1982).
4. J. P. GIROULT, M. GOREAUD, PH. LABBE, AND B. RAVEAU, *Acta Crystallogr. Sect. B* **37,** 2139 (1981).
5. B. DOMENGES, F. STUDER, AND B. RAVEAU, *Mater. Res. Bull.* **18,** 669 (1983).
6. B. DOMENGES, M. GOREAUD, PH. LABBE, AND B. RAVEAU, *J. Solid State Chem.* **50,** 173 (1983).
7. A. BENMOUSSA, D. GROULT, PH. LABBE, AND B. RAVEAU, *Acta Crystallogr. Sect.*, in press.
8. A. MAGNELI, *Acta Chem. Scand.* **2,** 861 (1948).
9. L. KIHLBORG, *Ark. Kemi* **21,** 35, 365 (1963).
10. A. J. SKARNULIS, E. SUMMERVILLE, AND L. EYRING, *J. Solid State Chem.* **23,** 59 (1978).
11. B. DOMENGES, thèse Docteur Ingénieur, Caen, Juillet (1983).
12. M. A. O'KEEFE AND S. V. SANDERS, *Acta Crystallogr. Sect. A* **31,** 307 (1975).
13. W. O. SAXTON AND M. A. O'KEEFE, "Electron Microscopy and Analysis," Inst. Phys. Conf. Ser. No. 61, Chap. 7, (1981).
14. L. A. BURSILL AND A. R. WILSON, *Acta Crystallogr. Sect. A* **33,** 672 (1977).